that was inclined by 15° from the horizontal plane is shown in Fig. 3. The speeds of the drops varied across the gradient and with the size of the drop; average speeds of 1 to 2 mm/s were observed for 1- to 2-μl drops on the steeper part of the gradient (*17*). The shape of the drop shown in Fig. 3 is that of a spherical cap. The difference of the contact angles in the advancing and receding edges of the drop was only ~2° to 3°. The effect of gravity on the drop shape was not significant here because the radius of the drop (1 to 1.5 mm) was smaller than the Laplace length (2.7 mm) (*18*). The near-spherical shape of the drop appears to be a consequence of the equilibration of the Laplace pressure inside the drop, which is consistent with the model proposed by Brochard (*3*).

Water was not the only liquid that moved across such gradient surfaces; other liquids such as glycerol and chloroform also moved. The motion of these liquids was, however, examined with a horizontal gradient surface.

Although we have not studied these factors in any detail, the speeds of the liquid drops depended on the hysteresis in contact angles, the surface tension and viscosity of the drops, the drop volume, the steepness of the gradient, and the inclination of the gradient surface. Detailed understanding of the kinetics of drop motion on gradient surfaces should take these factors into account. The gradient surfaces reported here are easily prepared. They should be useful in the study of the motion of liquid drops induced by chemical gradients and of the interplay of chemical and thermal gradients.

REFERENCES AND NOTES

1. H. Bouasse, *Capillarité et Phénomènes Superficielles* (Delagrave, Paris, 1924).
2. N. O. Young, J. S. Goldstein, M. J. Block, *J. Fluid Mech.* **6**, 350 (1959).
3. F. Brochard, *Langmuir* **5**, 432 (1989).
4. K. D. Barton and R. S. Subramanian, *J. Colloid Interface Sci.* **133**, 211 (1989).
5. A. W. Adamson, *Physical Chemistry of Surfaces* (Wiley, New York, ed. 3, 1976).
6. R. L. Cottington, C. M. Murphy, C. R. Singleterry, *Adv. Chem. Ser.* **43**, 341 (1964).
7. E. Raphael, *C. R. Acad. Sci. Paris Ser. II* **306**, 751 (1988).
8. T. Ondarcuhu and M. Veyssie, *J. Phys. (Paris) II* **1**, 75 (1991).
9. H. Elwing, S. Welin, A. Askendal, U. Nilsson, I. Lundstrom, *J. Colloid Interface Sci.* **119**, 203 (1987).
10. C.-G. Golander, Y.-S. Lin, V. Hlady, J. D. Andrade, *Colloids Surf.* **49**, 289 (1990).

11. These values of speed are approximate and variable. The effects of drop volumes on speeds have not been rigorously examined. Qualitatively, it was observed that the speeds increased as the volume of the drops increased.
12. Silicon wafers were cleaned in hot piranha solution, which is a mixture of 70% H_2SO_4 and 30% H_2O_2 (30% solution in water). The wafer was placed in this solution for 30 min. Afterward, the wafer was thoroughly rinsed with and stored in distilled water. Before we prepared the gradient surface, the wafer was rinsed again in running distilled water and then dried by blowing nitrogen over it.
13. We found that immersing the wafer in warm distilled water and rinsing it in pure distilled water helped to remove some of the loosely adsorbed contamination from the surface. The gradient surface can be easily contaminated by atmospheric impurities. The surface remained clean, however, when kept immersed in pure distilled water.
14. Drops used to measure the advancing and receding contact angles were held stationary on the surface of the silicon wafer by the tip of the microsyringe used to form the drops. The contact angles were measured under quasistatic conditions, that is, after the cessation of the movement of the contact line. For quantitative correlation between drop velocity and surface energy gradient, the contact angles should be measured under dynamic conditions. These measurements are beyond the scope of this study.
15. The thickness gradients of the monolayers were functions of the adsorption times and molecular weights of the silanes. We have also prepared gradient surfaces with $Cl_3Si(CH_2)_7CH_3$. After a 5-min adsorption, a close-packed, nearly complete monolayer (11 Å thick) was formed at the hydrophobic edge.
16. The thickness obtained by ellipsometry was an average over an area of ~3 mm^2.
17. The length (5 mm) of this gradient corresponds to what was detected by ellipsometry, which also matched the field of view of the telescope used to observe the motion of water drops. When the drop moved beyond 5 mm from the hydrophobic edge, the drop became flat and thin in the region of weaker gradient.
18. The Laplace length (also known as the capillary length) is $(\gamma_{LV}/\rho g)^{0.5}$, where ρ is the density of the liquid and g is the acceleration due to gravity.

19. M.K.C. acknowledges support from Dow Corning Corporation. G.M.W. acknowledges support from the Office of Naval Research and the Defense Advanced Research Projects Agency. We thank M. J. Owen (Dow Corning) for many valuable discussions.

9 January 1992; accepted 15 April 1992

Observation of Transition-State Vibrational Thresholds in the Rate of Dissociation of Ketene

Edward R. Lovejoy, Sang Kyu Kim, C. Bradley Moore

Rate constants for the dissociation of highly vibrationally excited ketene (CH_2CO) have been measured at the threshold for the production of $CH_2(^3B_1)$ and $CO(^1\Sigma^+)$. The rate constant increases in a stepwise manner with increasing energy, consistent with the long-standing premise that the rate of a unimolecular reaction is controlled by flux through quantized transition-state thresholds. The data give the energies of the torsional and C–C–O bending vibrations of the transition state.

The elementary chemical reaction is one of the most fundamental processes in nature, and the theoretical and experimental study of the transformation of reactants into products has been an important area of research for many decades. Experimental studies of unimolecular reactions of highly energized molecules provide strong tests of the theories developed to describe chemical reactivity (*1*). The unimolecular rate theory of Rice, Ramsperger, Kassel, and Marcus (RRKM) (*2*) is based on the assumptions that (i) the vibrational energy in the excited molecule is distributed statistically among all the vibrational degrees of freedom, (ii) the energy flows freely among the different degrees of freedom at a rate much faster than the reaction rate, and (iii) the rate of reaction is controlled by the passage through a transition state located at the dynamical bottleneck separating the reactant from products on the potential energy surface for the reaction. In the region of the transition state, the bound vibrational motions of the molecule are not coupled to the reaction coordinate, and passage through the transition state is vibrationally adiabatic. In this sense, the vibrational levels of the transition state represent reaction thresholds, that is, quantized channels connecting the reactant to products.

Chemical Sciences Division of the Lawrence Berkeley Laboratory and Department of Chemistry, University of California, Berkeley, CA 94720.

The energy dependence of the RRKM rate constant for a molecule with a fixed energy (E) and total angular momentum (J) is given by

$$k(E,J) = W^{\ddagger}(E,J)/[h\rho(E,J)] \qquad (3)$$

where $W^{\ddagger}(E,J)$ is the number of vibrational levels of the transition state with energy less than E, $\rho(E,J)$ is the density of vibrational states of the reactant (number of states per unit energy), and h is Planck's constant.

Definitive tests of RRKM theory are hampered by the difficulty in evaluating the individual terms in Eq. 1. Historically, the density of reactant states [$\rho(E,J)$] has been estimated by extrapolating a normal mode treatment of the molecular vibrations to higher energies (*3*). However, recent spectroscopic studies show that the actual density of states for a number of molecules is significantly higher (five to ten times for $10{,}000\ cm^{-1} < E < 30{,}000\ cm^{-1}$) (*4*) than predicted by the normal mode picture. The number of accessible reaction channels at

the transition state $[W^{\ddagger}(E,J)]$ is even more difficult to evaluate because of the lack of knowledge of the properties of the short-lived transition state. Generally, the vibrational frequencies of the transition state are estimated by extrapolating from the properties of the stable molecule. However, high-level quantum mechanical calculations now provide quantitative predictions for the properties of transition states of small molecules (5).

RRKM theory predicts that the rate constant increases by steps with an amplitude equal to $1/[h\rho(E,J)]$ as the energy of the reactant is increased through each vibrational state of the transition state. In the past, experiments have lacked the energy resolution and control of the angular momentum needed to resolve possible transition-state structure in the energy dependence of a rate constant. In this work, rate constants for the unimolecular dissociation of ketene were measured with an energy resolution much finer than the expected vibrational energy spacing at the transition state. The energy dependence of the rate constant exhibits clear steplike structures. Analysis of these structures provides a strong test of the basic tenets of unimolecular reaction rate theory.

The lowest energy dissociation channel for ketene yields triplet methylene [$CH_2CO \rightarrow CH_2(^3B_1) + CO(^1\Sigma^+)$] (Fig. 1) with a threshold 28,250 cm^{-1} above the zero point energy of ground-state ketene. There is a small barrier along the reaction coordinate (about 1300 cm^{-1} above the energy of the separated fragments), which controls the dynamics of the energy release to the separating fragments (6, 7). This barrier defines a distinct bottleneck to the reaction, and the triplet ketene decomposition represents a model case for testing RRKM theory.

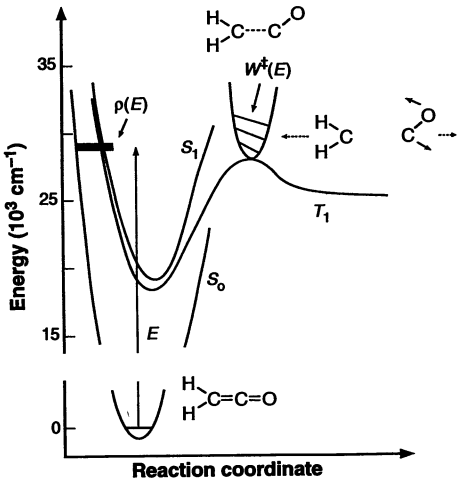

Fig. 1. A schematic representation of the dissociation of triplet ketene. The reaction coordinate corresponds to the distance between the carbon atoms. The solid lines represent the potential energy for the ground singlet (S_0), the first excited singlet (S_1), and the first triplet (T_1) electronic states. The transition state, which separates the highly vibrationally excited reactant from the products, is depicted as a single potential well perpendicular to the reaction coordinate. This well is meant to represent the eight bound vibrations of the transition state.

Highly vibrationally excited ketene was prepared by tunable pulsed laser excitation of ketene cooled in a supersonic jet expansion. Strong electronic-vibrational coupling in the energized molecule yields an excited state that is a statistical (8) mixture of the ground singlet (S_0), excited singlet (S_1), and triplet (T_1) states. The jet cooling (rotational temperature $\approx$ 5 K) and narrow bandwidth of the ultraviolet excitation laser (0.4 cm^{-1}) minimized the uncertainty in the energy and angular momentum of the excited molecules.

We measured rate constants for the unimolecular decomposition of ketene by monitoring the appearance of the CO (vibrational level $v = 0, J_p = 12$) fragment as a function of time after ketene excitation. The CO photofragment was detected by vacuum ultraviolet laser-induced fluorescence (LIF). The experimental conditions and data treatment are as described (6, 7). Rate constants were measured at energy increments of 2 to 4 cm^{-1}, and the measurements were repeated over the entire energy range three times. The average dissociation rate constant (Fig. 2, curve a) exhibits clear steps in the first few hundred wave numbers above an initial step associated with the zero point vibrational level of the transition state.

Photofragment excitation (PHOFEX) spectra of the CO product were also taken. The LIF signal from specific $CO(v,J_p)$ rovibrational states was measured at a fixed reaction time (Δt) as a function of the ketene excitation energy (E). The PHOFEX signal can be expressed as

$$S(E,v,J_p,\Delta t) \propto \sigma(E)\, P(E,v,J_p)\, (1 - e^{-k(E)\,\Delta t}) \quad (4)$$

where $\sigma(E)$ is the ketene absorption cross section, $P(E,v,J_p)$ is the yield or branching ratio for the (v,J_p) quantum state of CO, and $k(E)$ is the ketene dissociation rate constant. The absorption cross section is unstructured at the energies accessed in this study and does not contribute significantly to the structure in the PHOFEX spectra. For small reactive conversion [$k(E)\,\Delta t << 1$], the PHOFEX signal is proportional to the rate constant and the $CO(v,J_p)$ yield.

The PHOFEX spectrum of $CO(v = 0, J_p = 12)$ at 50 ns (Fig. 2, curve b) shows clear steps that match those in the rate constant. A plot of $(1 - e^{-k(E)\,\Delta t})$ based on the experimental $k(E)$ data and a reaction time of 50 ns is shown in Fig. 2, curve c. There is a strong correspondence between this simulated PHOFEX spectrum and the experimental spectrum for $E < 28{,}500$ cm^{-1}, indicating that the PHOFEX structure for the $CO(v = 0, J_p = 12)$ state is dominated by the variation of the rate constant with excitation energy. The abrupt change in slope of the $CO(v = 0, J_p = 12)$ PHOFEX spectrum at 28,500 cm^{-1} reflects a sudden decrease in the fractional yield of $J_p = 12$. The rate constant continues to rise sharply in this region. The PHOFEX spectrum of the $CO(v = 0, J_p = 2)$ product (Fig. 2, curve d) is significantly different, suggesting that the energy dependence of the $CO(v = 0, J_p =$

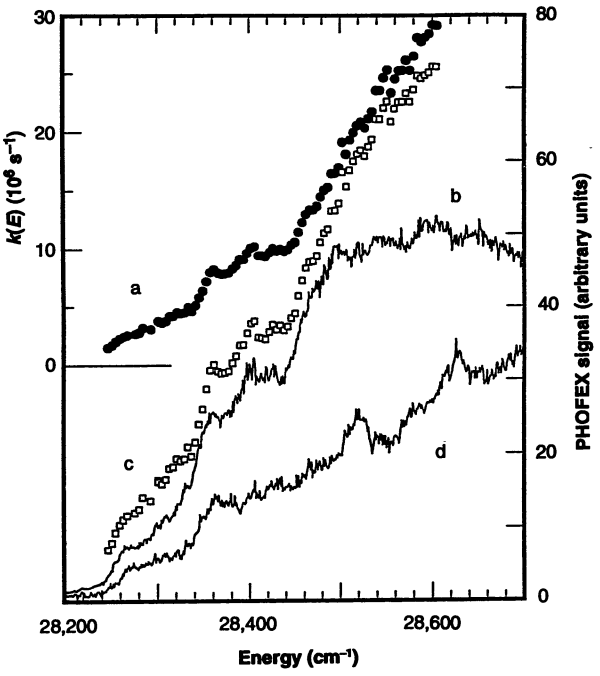

Fig. 2. CH_2CO dissociation rate constant and PHOFEX data. Curve a, experimental rate constants for the unimolecular decay of ketene. Curve b, $CO(v = 0, J_p = 12)$ PHOFEX signal. Curve c, PHOFEX spectrum calculated from the experimental rate constant data. Curve d, $CO(v = 0, J_p = 2)$ PHOFEX signal. The actual ratio of the yields of $CO(v = 0, J_p = 12)$ to $CO(v = 0, J_p = 2)$ is about 20:1 at 28,500 cm^{-1} for CH_2CO (7).

2) yield contributes to the structure in the PHOFEX spectrum of the low-J product.

The CD_2CO decomposition rate constant (Fig. 3, curve a) increases in a distinct stepwise pattern with increasing energy, but with smaller energy spacing between the steps as compared to that observed for CH_2CO. The narrower spacing is consistent with the expected decrease in the vibrational frequencies of the transition state upon isotopic substitution. The PHOFEX spectrum for the CO(v = 0,J_p = 12) product from CD_2CO at 200 ns, and a spectrum calculated from the $k(E)$ data are shown in Fig. 3, curves b and c, respectively. As is the case for CH_2CO, the CO(v = 0,J_p = 12) and simulated spectra are very similar, suggesting that the structure in the CO(v = 0,J_p = 12) PHOFEX spectrum is attributable predominantly to the structure in the CD_2CO rate constant. A PHOFEX spectrum of the CO(v = 0,J_p = 2) product from the dissociation of CD_2CO at a delay time of 150 ns is shown in Fig. 3, curve d. Similar to the results for CH_2CO, additional sharp features are observed in the low-J_p PHOFEX spectrum for CD_2CO, indicating that the energy dependence of the low J_p CO yield is structured.

Allen and Schaefer have performed sophisticated quantum mechanical calculations for the dissociation of triplet ketene (9). The calculations describe a transition state that has a strongly bent C–C–O framework [about 116° versus 180° (linear) for the ground state] and a C–C bond that is extended by about 40% relative to the ground state. The lowest frequency vibrations at the transition state are the torsion between the CH_2 and CO portions of the molecule, the C–C–O bend (252 cm^{-1}), and the CH_2 wag (366 cm^{-1}). The torsional motion is a hindered internal rotation with an ab initio barrier of 380 cm^{-1}. The ab initio CH_2CO hindered rotor potential gives a spacing of about 140 cm^{-1} between the first two states, which is larger than the spacing between the first two steps in the data. The calculated hindered rotor spacing for CD_2CO is about 20% lower than for CH_2CO, which is in good agreement with the fractional difference in the energy spacings of the first two steps in the data for CH_2CO and CD_2CO.

A significant fraction (0.22) of the potential energy released as the CH_2 and CO fragments repel each other appears as rotational energy of the CO fragment, consistent with the strongly bent C–C–O geometry of the transition state and rapid release of the energy along the C–C bond (7). The angular momentum imparted to the CO is reproduced very well by a simple classical model that assumes that the available energy is released impulsively along the C–C bond at the transition state. This model predicts only the fraction of energy released to rotation (that is, only one J_p value for CO) and not the distribution of angular momentum. The shapes of the CO rotational distributions are derived from the vibrational motion of the molecule when the C–C bond breaks (7). This dynamical model predicts that each vibrational state of the transition state, with its characteristic motion, gives a unique distribution of angular momentum in the products. The variation in the CO(v,J_p) yield with energy is reflected in the PHOFEX spectra. Therefore, these spectra contain detailed information about the vibrational character of the transition-state thresholds.

For example, the CO(v = 0,J_p = 2) PHOFEX spectrum exhibits two sharp features at about 28,500 and 28,600 cm^{-1} which are absent from the CO(v = 0,J_p = 12) spectrum but which correlate with the sudden change in slope in the CO(v = 0,J_p = 12) spectrum. The prominence of these features in the low J_p spectrum indicates that the transition state thresholds at these energies involve atomic motions that enhance the production of CO in low J_p states. The spacing between these features is comparable to the spacing between the first two pronounced steps in the PHOFEX spectra, suggesting that the states are combinations of the lowest energy hindered rotor states with an excited state of a different vibrational mode. The excited (v = 1) C–C–O bend is a likely assignment for these thresholds because the bending motion adds or subtracts significant angular momentum from the impulsive release and broadens the CO J_p distribution. The broadening increases the yield of low J_p products and decreases the yield of J_p states near the maximum of the distribution ($J_p \approx 12$). This assignment gives a C–C–O bending energy of 250 ± 10 cm^{-1} at the transition state, which agrees very well with the ab initio value of 252 cm^{-1} (9).

The dissociation rate for deuterated ketene is significantly slower than for the hydrogen isotopomer, because the deuterated compound has a larger density of reactant states [$\rho(E,J)$] owing to its reduced vibrational frequencies. The rate constant measured at the top of the second prominent step for CH_2CO (28,360 cm^{-1}) is 4.0 ± 0.8 times the CD_2CO rate constant at the same position (28,410 cm^{-1}), suggesting that the CD_2CO density of states is four times the CH_2CO state density at these energies. The ratio of harmonic state densities (3) is 3.6:1. The absolute density of reactant states is difficult to evaluate because of uncertainties in the number of transition-state levels that contribute to each step in the rate constant (10).

The observation of steps in the rate constant supports the concept that the rate of a unimolecular reaction with a well-defined barrier (and hence transition state) is controlled by flux through quantized transition-state thresholds. Results for the dissociation of singlet ketene (11) show that it remains much more difficult to define the transition state and the dynamics of energy flow for reactions without barriers. The comparison of experimental and ab initio data given here also demonstrates that many properties of the transition state are predicted by theory.

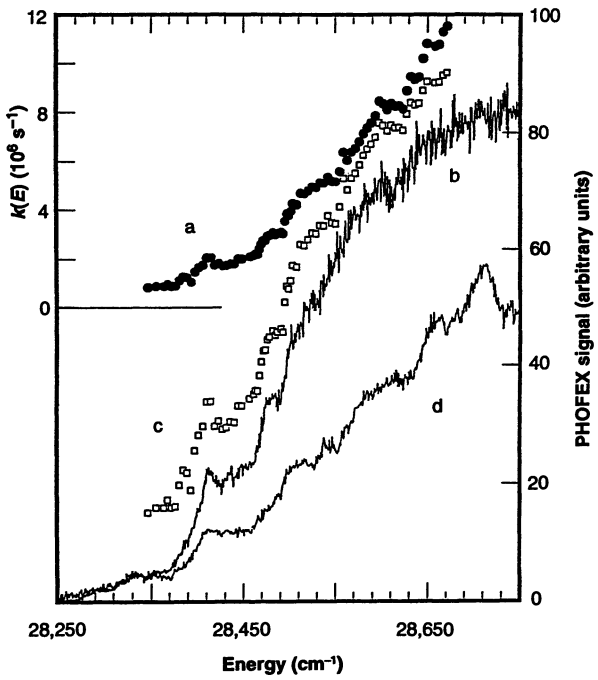

Fig. 3. CD_2CO data (see legend to Fig. 2).

REFERENCES AND NOTES

1. For reviews, see: F. F. Crim, *Annu. Rev. Phys. Chem.* **35**, 657 (1984); H. Reisler and C. Wittig, *ibid.* **37**, 307 (1986).
2. R. A. Marcus and O. K. Rice, *J. Phys. Colloid Chem.* **55**, 894 (1951); R. A. Marcus, *J. Chem. Phys.* **20**, 359 (1952); W. Forst, *Theory of Unimolecular Reactions* (Academic Press, New York, 1973).
3. G. Z. Whitten and B. S. Rabinovitch, *J. Chem. Phys.* **38**, 2466 (1963).
4. E. Abramson, R. W. Field, D. Imre, K. K. Innes, J. L. Kinsey, *ibid.* **83**, 453 (1985); W. F. Polik, D. R. Guyer, C. B. Moore, *ibid.* **92**, 3453 (1990); A. Geers, J. Kappert, F. Temps, W. Wiebrecht, *Ber. Bunsenges. Phys. Chem.* **94**, 1219 (1990); Y. S. Choi and C. B. Moore, *J. Chem. Phys.* **94**, 5414 (1991).
5. C. E. Dykstra, *Annu. Rev. Phys. Chem.* **32**, 25 (1981); C. W. Bauschlicher, S. R. Langhoff, P. R. Taylor, *Adv. Chem. Phys.* **77**, 103 (1990).
6. I.-C. Chen and C. B. Moore, *J. Phys. Chem.* **94**, 263 (1990).
7. ———, *ibid.*, p. 269.
8. The character of the excited state is mostly that of highly vibrationally excited ground singlet because of the overwhelming density of ground singlet states at these energies. The harmonic densities of vibrational states are 1.2×10^4 (S_0), 15 (S_1), and 60 (T_1) per cm^{-1} at 28,250 cm^{-1} above the S_0 zero point level.
9. W. D. Allen and H. F. Schaefer III, *J. Chem. Phys.* **89**, 329 (1988).
10. An upper limit for the density of CH_2CO states can be calculated by assuming that the first two rate constant steps represent two hindered rotor levels, which are each triply degenerate as a result of the electron spin. If this is the case, the density of CH_2CO states is 4.5×10^4 per cm^{-1} at 28,360 cm^{-1}, which is about four times the harmonic count.
11. S. J. Klippenstein and R. A. Marcus, *J. Chem. Phys.* **93**, 2418 (1990); W. H. Green, Jr., A. J. Mahoney, Q.-K. Zheng, C. B. Moore, *ibid.* **94**, 1961 (1991).

12. Supported by the Director, Office of Energy Research, Office of Basic Energy Sciences, Chemical Sciences Division of the U.S. Department of Energy under contract DE-AC03-76SF00098.

6 February 1992; accepted 21 April 1992

Mechanism of the Rhodium Porphyrin–Catalyzed Cyclopropanation of Alkenes

Jana L. Maxwell, Kathlynn C. Brown, David W. Bartley, Thomas Kodadek*

The rhodium porphyrin–catalyzed cyclopropanation of alkenes by ethyl diazoacetate (EDA) is representative of a number of metal-mediated cyclopropanation reactions used widely in organic synthesis. The active intermediate in these reactions is thought to be a metal carbene complex, but evidence for the involvement of metal-olefin π complexes has also been presented. Low-temperature infrared and nuclear magnetic resonance spectroscopies have been used to characterize a rhodium porphyrin–diazoalkyl adduct that results from the stoichiometric condensation of the catalyst and EDA. Optical spectroscopy suggests that this complex is the dominant steady-state species in the catalytic reaction. This compound decomposes thermally to provide cyclopropanes in the presence of styrene, suggesting that the carbene is indeed the active intermediate. Metal-alkene π complexes have also been detected spectroscopically. Kinetic studies suggest that they mediate the rate of carbene formation from the diazoalkyl complex but are not attacked directly by EDA.

The design of asymmetric catalysts for use in synthesis has emerged as one of the most important problems in modern organic chemistry because most biologically active compounds are chiral. Recently, there has been a great deal of interest in the development of metal-based asymmetric cyclopropanation catalysts (*1*) for the synthesis of pyrethroid insecticides, β-turn peptide mimics, and a number of other interesting compounds. We have concentrated on rhodium porphyrin catalysts and have developed moderately enantioselective systems for the cyclopropanation of alkenes by diazo esters. In order to rationally design more effective asymmetric pockets, it is important to understand in detail the mechanism of the reaction, including the nature of the reactive intermediates and the arrangement of atoms in the transition state. This will allow a rational positioning of groups in the chiral cavity to more effectively influence the approach of the prochiral substrate to the metal. Unfortunately, despite considerable investigation, many aspects of the mechanism of metal-catalyzed cyclopropanations remain unclear. Current speculation is that the catalyst reacts with the diazo compound to produce an electrophilic metal carbene that is subsequently attacked by the alkene to provide the cyclopropane and regenerate the catalyst (Eq. 1) (*2*).

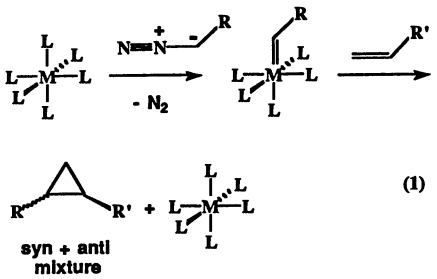

(1)

However, a carbene complex has never been observed in a catalytic system (*3*). An alternative mechanism that has been discussed is nucleophilic attack of the diazo compound on a metal-alkene π complex (Eq. 2) (*4*).

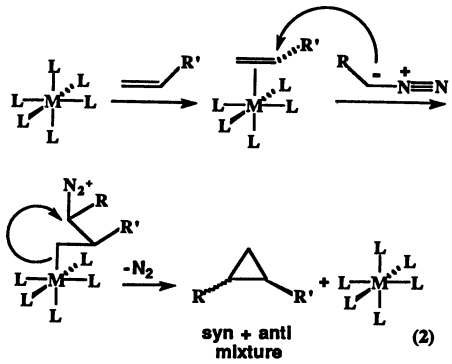

(2)

Nucleophilic additions to metal-alkene complexes are common in organometallic chemistry (*5*), and π complexes have been characterized for some cyclopropanation catalysts (*4*). However, the precise role of these species is unclear. Other mechanisms are also possible. We report a mechanistic analysis of the rhodium porphyrin–catalyzed cyclopropanation of alkenes by ethyl diazoacetate (EDA) (*6*) that clarifies these matters. Our results, including the characterization of a reactive organometallic intermediate, provide strong evidence for the intermediacy of a metallocarbene and also reveal a novel role for the substrate as an axial ligand that moderates the rate of carbene formation when the catalyst has a labile ligand such as iodide.

In order to probe for the possible formation of a reactive rhodium porphyrin carbene, we investigated the stoichiometric reaction of EDA with a rhodium porphyrin in the absence of alkene. Addition of a slight excess of EDA to a CD_2Cl_2 solution of iodorhodium tetra(*p*-tolyl) porphyrin (RhTTPI) at −40°C results in a rapid, subtle color change and formation of a porphyrin-EDA adduct. The ^1H nuclear magnetic resonance (NMR) spectrum of this species exhibits a single set of resonances attributable to the protons of the EDA-derived fragment (Fig. 1). Each signal is shifted upfield relative to its position in EDA, demonstrating that these protons sit above the face of the aromatic macrocycle, which has a strong diamagnetic ring current. The proton α to the carbonyl carbon is a doublet, although a two-dimensional correlated (2-D COSY) spectrum shows that it is not coupled to any other proton. Therefore, the splitting is due to coupling

Department of Chemistry and Biochemistry, University of Texas at Austin, Austin, TX 78712.

*To whom correspondence should be addressed.